Journal of Russian Laser Research, Volume 19, Number 2, 1998

PHOTOASSOCIATION SPECTROSCOPY: DETERMINATION OF PARAMETERS OF POTENTIALS OF DIATOMIC MOLECULES

J. G. Eden,[1] H. T. Tran,[1] and V. S. Zuev[2]

[1] *Everitt Laboratory, University of Illinois at Urbana-Champaign, 1406 West Green Street, Urbana IL 61801, USA*

[2] *P. N. Lebedev Physical Institute, Russian Academy of Sciences, Leninskii Pr. 53, Moscow 117924, Russia*

Abstract

Laser-induced fluorescence studied with the help of a tunable dye laser is used to record the photoassociation spectrum of equilibrium mercury atoms in the range of 34 700–37 300 cm^{-1}. The so-called Franck–Condon structure, which represents periodic variations of absorption intensity on a continuous background, is observed. The structure makes it possible to determine spectroscopic parameters of the upper bound potential and the lower repulsive potential, including the potential with a shallow Van der Waals well. The Numerov–Cooley procedure is used to find the numerical solution of the boundary problem, namely, eigenfunctions and eigenvalues of the Schrödinger equation for the one-dimensional motion in a potential field, matrix elements of transitions and partial waves, and the absorption spectrum of collisional pairs of atoms are calculated. The absorption spectrum of mercury dimers was simulated taking into account 100 vibrational and 200 rotational levels. The comparison of theoretical and experimental spectra according to Tellinghuisen made it possible to determine the lower part of the potential curve for the dimer excited state.

In the case where one of the energy levels of a molecule changing its electronic state belongs to the continuum, this transition is termed the free-bound transition. The corresponding spectra are continuous in contrast to the spectra with sharp rotational lines and sharp edges of vibrational bands (bound-bound transitions). However, continuous spectra also have a noticeable structure in the form of intensity variations on a continuous background. The structure is caused by variations of the Franck–Condon factor, the square of the overlap integral for the wave functions of molecular states involved in the process, with the change of transition frequency.

Structure continuous spectra can be quantitatively analyzed by comparing with spectra obtained in a calculation experiment. This gives data on energy eigenvalues, vibrational and rotational constants, and molecular potentials. The potentials found by this analysis are rather reliable even in comparison with the potentials found by the Rydberg–Klein–Rees method from band molecular spectra.

The fruitfulness of studying structure continuous spectra was analyzed in detail in [1]. It should be noted that the analysis of the effect consisting in the spectral structure formation in the case of bound-free transitions, which is now referred to as the internal Condon diffraction, can be found in the early paper [2], which is cited as the pioneer work concerning the Franck–Condon principle.

Excimer molecules form a class of diatomic molecules having a repulsive ground state and a bound excited electronic state. Bound-free radiative transitions in these molecules represent an example of continuous molecular spectra.

It is common to produce excited excimer molecules either in chemical reactions of excited atoms or ions due to excitation with electrons of a discharge or a beam or through photodissociation of polyatomic molecules. In an experiment with excimer molecules, the fluorescence spectrum corresponding to transitions from excited bound electronic states to the ground repulsive state is recorded. The experimental results are compared with the calculated spectrum. The main problem is associated with the vibrational distribution of excited

Translated from Preprint No. 71 of the P. N. Lebedev Physical Institute, Moscow, 1997.

1071-2836/98/1902-0116$20.00

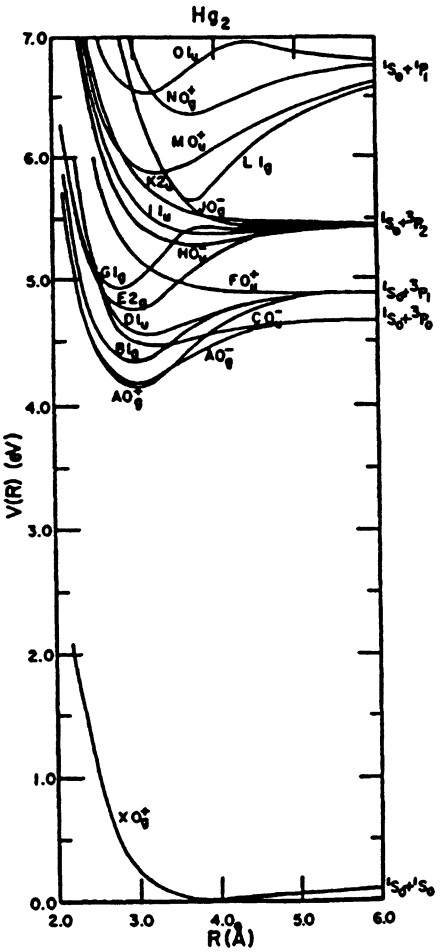

Fig. 1. Diagram of electronic states of the Hg_2 molecule.

molecules. If the rate of V–T relaxation is insufficiently large in comparison with the radiative process, one should carry out a special study to determine the vibrational distribution. If the rate of V–T relaxation is sufficiently large, the spectrum contains information only on vibrational levels with small vibrational numbers, i.e., the levels that are thermally excited.

A new situation arises in the case where a free-bound transition is excited with photons. Free pairs of atoms with certain internuclear distances and kinetic energy can absorb photons and thus change to bound states of corresponding molecules. This absorption, which is associated with a free-bound transition, is known as pressure-induced absorption (see, e.g., [3] and the references therein) or absorption due to photoassociation. It can be used as an alternative method of studying excimer molecules.

It is more convenient to measure the fluorescence excitation spectrum under conditions of photoassociation and not the absorption spectrum. In this case, it is possible to observe free-bound transitions with photon absorption and a change to virtually all vibrational levels, including very high levels. Carrying out an experiment at a sufficiently high pressure, which is so high that molecules found in an excited bound state undergo V–T relaxation before the emission event, and detecting fluorescence of molecules at a fixed frequency from strongly emitting lower vibrational levels, one records the excitation spectrum. If the relaxation over vibrational levels is identical for all excitation wavelengths, the fluorescence excitation spectrum is equivalent to the absorption spectrum.

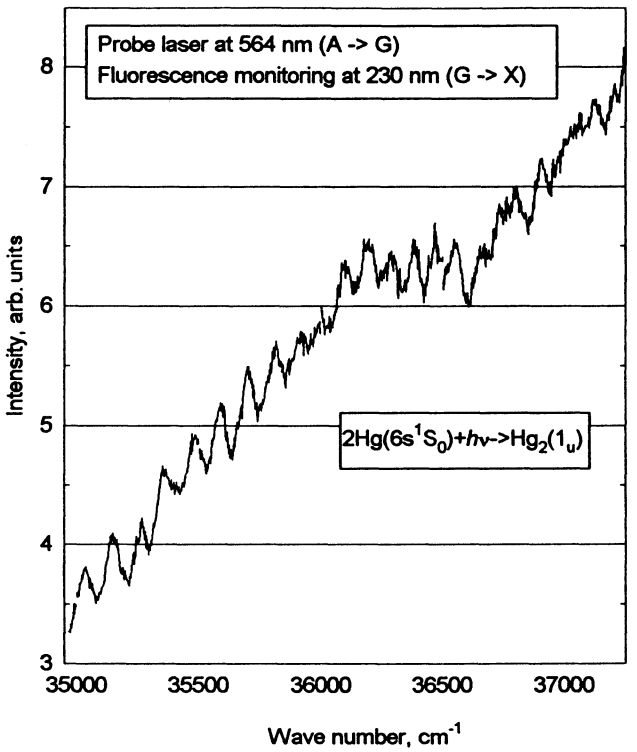

Fig. 2. Photoassociation spectrum for Hg–Hg pairs of atoms.

The above method was developed and described in [4–8], in particular, for the Kr–F and Xe–I pairs of atoms and the KrF and XeI molecules. These papers present references to the works that formed the basis of the method.

The instruments and technique used in these experiments are the following [7]. Initially a pulse of an auxiliary laser produces free halogen atoms through photodissociation of F_2 or I_2. The main laser is switched on with a time delay. This laser is frequency tunable and its radiation causes photoassociation of Kr–F or Xe–I collisional pairs of atoms, which produces molecules on a certain vibrational level of an excited electronic state of a molecule, more specifically, the $B^2\Sigma^+_{1/2}$ state. Subsequent collisional relaxation over vibrational levels results in fluorescence from lower vibrational levels of the state B. The excitation spectra are obtained by recording the fluorescence intensity in the course of laser frequency tuning. The results of observation and analysis of photoassociation spectra for the Kr–F and Xe–I pairs of atoms, including the determination of parameters of potential curves, are presented in [4-8].

Excimer molecules include Hg_2, the mercury dimers, which have the repulsive ground state $X0^+_g$ with a shallow Van der Waals well, with a internuclear distance of about 0.37 nm. The Hg_2 molecules are the subject of our present study.

Figure 1 illustrates the diagram of electronic states of the Hg_2 molecule. Photoassociation of collisional Hg–Hg pairs takes place under irradiation with wavelength of 268–288 nm and corresponds to the $X0^+_g \rightarrow D1_u$ transition. The $Hg_2(D)$ molecules formed in the process undergo collisional relaxation to the nonradiative $A0^+_g$ state. Later on, these molecules are exposed to radiation with wavelength of 564 nm and make the $A0^+_g \rightarrow G0^+_u$ transition. Subsequently, the $Hg_2(G)$ molecules make a radiative transition to the ground state. The intensity of laser-induced fluorescence corresponding to the $G0^+_u \rightarrow X0^+_g$ transition and observed in the

range of 210–240 nm is measured as a function of radiation wavelength of the first laser. This gives the photoassociation spectrum for collisional pairs of mercury atoms.

In the experiment, mercury vapors are heated to a temperature of 300–320 °C. The density of saturated mercury vapors at this temperature is equal to $(3.6\text{–}7.2)\cdot 10^{18}$ cm^{-3} (it is calculated using the data on pressure from [9]). At this temperature, mercury vapors represent a monatomic gas. The depth of the Van der Waals well is about 400 cm^{-1}, and kT has approximately the same value. In view of this fact, the Van der Waals molecules are almost totally dissociated because of the large statistical weight of a free atomic state.

Figure 2 presents the experimental photoassociation spectrum for Hg–Hg atoms, which is recorded in the way described above. One can clearly see intensity oscillations on a continuous background whose level increases with increasing wave number.

It is common to derive information from photoassociation spectra by the iteration method, which is based on the comparison of calculated and experimental spectra. The values of parameters of potentials involved in the problem are obtained by fitting the calculated spectrum to the experimental one. The procedure calls for multiple calculations with a variable functional form of potentials and different values of variable parameters. In actuality, one solves the inverse problem. The question of procedure uniqueness is a subject of a special study, which is beyond the framework of our present work.

The contributions of different transitions in the continuum will be summed using the rule adopted in [7]. The photoassociation absorption coefficient k_{PA} will be assumed to be proportional to the quantity

$$k_{\text{PA}} \sim \nu S(\nu) N_{\text{Hg}}^2, \tag{1}$$

where

$$S(\nu) = \sum_{\nu', J} P_{\nu' J}(\varepsilon''_J), \tag{2}$$

where, in turn,

$$P_{\nu' J}(\varepsilon''_J) = (2J+1)\exp\left(-\frac{\varepsilon''_J}{kT}\right)\left|\langle\psi_{\nu' J}|\mu(R)|\psi_{\varepsilon''_J}\rangle\right|^2. \tag{3}$$

Here, $P_{\nu' J}(\varepsilon''_J)$ is the so-called partial wave. The first and second factors on the right-hand side are the rotational statistical weight and the Boltzmann factor.

Strictly speaking, the energy distribution of pairs of mercury atoms in a closed space with a potential maximum must be different from the distribution in a space without a potential maximum. This is caused by the dependence of the degeneracy multiplicity for a state with a given energy on the energy value. By analogy with the data for Xe_2 [10], we assume that this difference is small. Because of this, the Boltzmann factor used in (3) has no corrections. Moreover, we do not discriminate between the rotational branches P, Q, and G. In (3), the rotational number J is given without a subscript specifying the state, the upper or the lower one. The rotational structure of the spectrum is taken into account with the help of one branch, namely, the Q branch.

The calculation of the spectrum is reduced to the calculation of wave functions and squares of matrix elements $\left|\langle\psi_{\nu' J}|\mu(R)|\psi_{\varepsilon''_J}\rangle\right|^2$. The wave functions $\psi_{\nu' J}$ and $\psi_{\varepsilon''_J}$ are found with the help of the functions $\phi_{\nu' J}/R$ and $\phi_{\varepsilon''_J}/R$, which are eigenfunctions of the one-dimensional Schrödinger equation

$$\frac{d^2\phi(R)}{dR^2} + \frac{8\pi^2\mu}{h^2}\left[E - U_0(R) + \frac{h^2}{8\pi^2\mu R^2}J(J+1)\right]\phi(R) = 0, \tag{4}$$

where energy is measured in energy units.

It is known that (4) is the equation to which the problem of particle motion in a centrally symmetric field is reduced. In view of the restrictions imposed by symmetry, we must deal with the $^1\Sigma - ^1\Sigma$ transitions,

and these particular transitions will be considered below. In (4), $\mu = \dfrac{m_1 m_2}{(m_1 + m_2)N_A}$ is the reduced mass of a molecule, where m_1 and m_2 are the masses of atoms comprising a molecule (in atomic units), and $N_A = 6.0221 \cdot 10^{23}$ mol^{-1} is the Avogadro number, which is used to express the reduced mass in grams.

By analogy with [4–8], Eq. (4) will be numerically integrated using the Numerov–Cooley algorithm [11, 12]. Equation (4) with the boundary conditions

$$\phi(0) = 0 \quad \text{with } \phi(R) \text{ limited,}$$

is replaced with the difference equation

$$Y_{i+1} + Y_{i-1} - 2Y_i = h^2(U_i - E)\phi_i, \tag{5}$$

where

$$Y_i = \left[1 - \frac{h^2}{12}(U_i - E)\right]\phi_i. \tag{6}$$

Here

$$\begin{aligned} R_i &= R_0 + ih, \quad i = 0, 1, 2, \ldots, n+1, \\ \phi_i &= \phi(R_i), \\ U_i &= U(R_i), \end{aligned} \tag{7}$$

$$U(R) = \frac{8\pi^2\mu}{\hbar^2} U_0(R) + \frac{J(J+1)}{R^2}. \tag{8}$$

In (6) and (7), h is the R step; in (8), $\hbar$ is the Planck constant.

For $E > U(\infty)$, which corresponds to the motion of atoms in a molecule that is bounded from one side only, the solution to Eq. (4) exists for all E. It can be found with the help of formula (5). Note that one should begin with the following values:

$$\phi_0 = 0, \quad \phi_1 \text{ is an arbitrarily small number.}$$

If $E < U(\infty)$, solutions to Eq. (4) exist only for discrete values of E.

The condition of limitedness of an eigenfunction of Eq. (4) for any R is equivalent to the conditions

$$\begin{aligned} &\phi_{n+1} \text{ is an arbitrarily small number,} \\ &\phi_n = \phi_{n+1} \exp\left(R_{n+1}\sqrt{U_{n+1} - E} - R_n\sqrt{U_n - E}\right). \end{aligned} \tag{9}$$

The second condition in (9) is the result of the assumption that the potential $U(R)$ for R_n changes negligibly on the de Broglie wavelength, which makes it possible to calculate the wave function in the WKB approximation (the quasi-classical approximation).

To carry out numerical integration of Eq. (4), one should have preliminarily (approximate) values of energy eigenvalues. If the preliminarily value of E is set with insufficient accuracy, the program omits some eigenvalues, and the other eigenvalues are recalculated. Preliminary values are the subject of program automation and will not be discussed here in greater detail. When plotting the dependence of E on n, the number of energy eigenvalues, one usually sees from perturbations of monotonicity of the curve in what direction the preliminary energy value should be changed in order to find the omitted value.

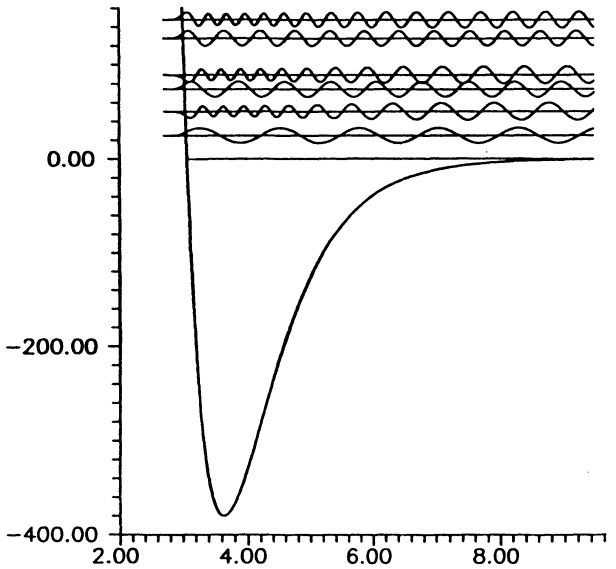

Fig. 3. Wave functions for the potential with a well and the purely repulse potential. The abscissa is the internuclear distance in angstroms, and the ordinate is the energy in cm^{-1}.

For a certain preliminary value of E, the eigenfunction is calculated starting with R_0, which is found reasonably far to the left of the repulsive branch of the potential curve. The first two values of the eigenfunction should be chosen in the form

$$\phi_0 = 0, \quad \phi_1 \text{ is an arbitrarily small number.}$$

The integration is performed up to a certain point R_m, which is arbitrarily specified on the interval between the repulsive and attractive branches of the potential curve $U(R)$. In view of the fact that Eq. (4) is inhomogeneous with respect to ϕ, the quantities ϕ_i may be replaced with $\phi_i^{\text{out}} = \phi_i/\phi_m$, where $i = 1, 2, 3, \ldots, m$. Further on, one uses (9) and (5) and performs integration from R_{n+1} to $R_m < R_{n+1}$, which gives the quantities ϕ_i^{in}, where $i = n+1, n, \ldots, m$. It is natural that the solutions calculated at the point R_m are equal to each other

$$\phi_m^{\text{out}} = \phi_m^{\text{in}} = 1;$$

however, the derivatives do not coincide. The difference between the values of derivatives makes it possible to determine the correction (see [11]) to the energy eigenvalue expectancy by the formula

$$D(E) = \frac{(-Y_{m-1} + 2Y_m - Y_{m-1})\,h^{-2} + (U_m - E)\,\phi_m}{\sum\limits_{i=1}^{n} \phi_i^2}. \tag{10}$$

The procedure is repeated and it suffices, as a rule, to make five or six iterations in order that the correction be smaller than a small value chosen in advance. According to [12], the program may show oscillations, but we have not observed this effect.

The wave functions are normalized. The functions of the discrete energy spectrum are normalized in such a way that the integral of the wave function squared taken over the coordinates is equal to unity. The functions of the continuum are normalized so that the integral of the wave function squared over all possible values of energy is equal to unity. In view of the absence of Van der Waals molecules, there is no need to

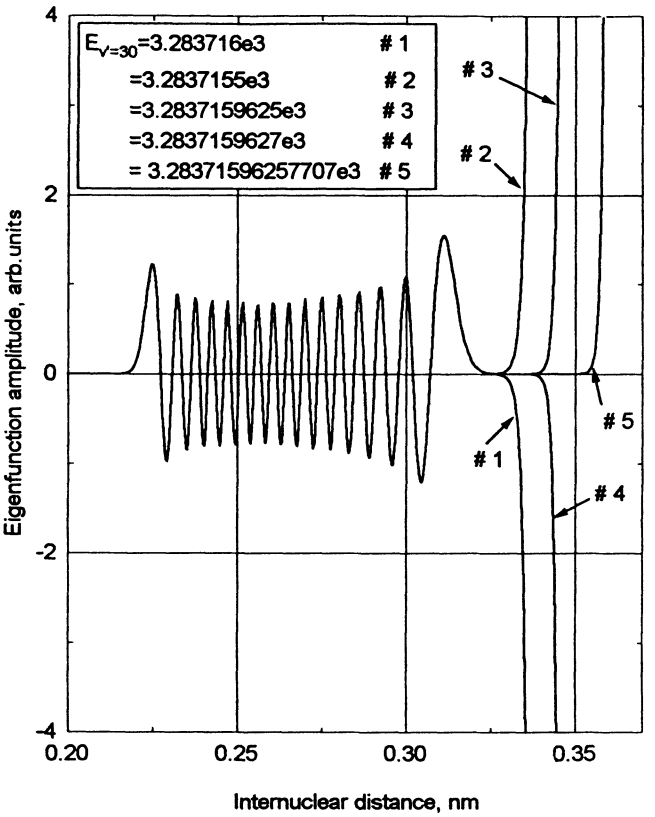

Fig. 4. Illustration of the instability of the Numerov–Cooley algorithm.

calculate wave functions of the lower state in the discrete spectrum. It is natural that these calculations should be performed for decreased temperatures of mercury vapors.

We shall use the procedure of derivation of intermediate results with the help of the program developed for the calculation of photoassociation spectrum in order to illustrate the role of different effects. This seems to be useful from the methodological point of view. In some case, we shall obtain illustrations to [13] concerning the role of kinetic energy in the Franck–Condon principle.

The presence of a potential well in the potential curve of the lower state has a crucial effect on the wave functions of the lower state. One can see this effect in Fig. 3, where two potential curves are presented on a large scale. One potential curve has a potential well with depth of about 400 cm^{-1}, and the other curve has no potential well. The curves coincide for $E > 0$. At the point $E = 0$, the second curve changes to the horizontal straight line.

Six wave functions shown above the level $E = 0$ were calculated in pairs for three approximately equal energy values, but for different potentials. The plots of wave functions are placed on the corresponding energy levels. Each upper wave function in a pair is calculated for the potential with a well, and the lower functions are calculated for the potential without a well. One can see that the spatial period of the corresponding wave functions above the potential well (it may be referred to as the de Broglie wavelength) is noticeably decreased because of the kinetic-energy excess (momentum excess) in comparison with the case of motion in the potential without a well. Thus, the potential well in the lower curve gives no contribution to the form of the line spectrum, but changes wave functions and the corresponding overlap integrals (the Franck–Condon factor). As a result, the photoassociation is changed, too.

Figure 4 illustrates the wave function for the vibrational number $\nu' = 30$. The right-hand side of this

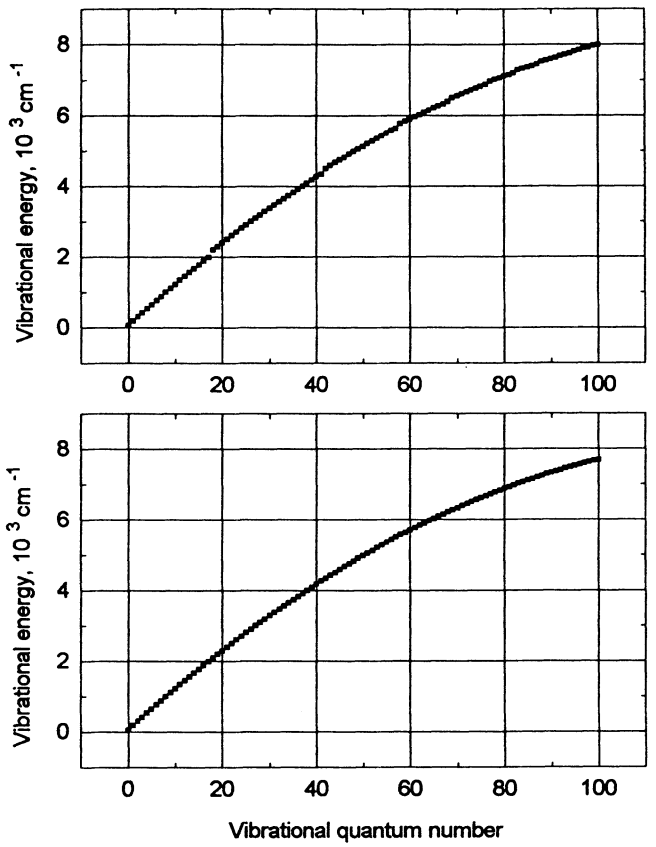

Fig. 5. The dependence of the vibrational-energy eigenvalue on the vibrational number.

picture illustrates the stability and the accuracy of the Numerov–Cooley algorithm. The point is that in actuality the figure presents five wave functions, which are calculated by integration from a small R_0 in the direction of increasing R without the use of the corrector–predictor formula (10), but for the values of E that are rather close to the eigenvalue $E = E_{\nu'=30}$. The corresponding values are presented in the figure. They should be enumerated in the order of 1–5 from the top to the bottom. The energy (in cm^{-1}) is measured from the bottom of the potential well. The closer the value of E to the eigenvalue, the longer the wave function remain limited (curves 1–5).

The curve in the upper fragment of Fig. 5 illustrates (in the form of bends of the curve) the aforementioned effect of loss of some eigenvalues during the calculation. The preliminary energy values were specified with insufficient accuracy. The curve in the lower part of the curve has no bends, i.e., we found all eigenvalues and none of them was missed.

When formulated classically (we mean classical mechanics), the Franck–Condon principle means exact conservation of coordinates and momenta of nuclei of atoms, which form a diatomic molecule, during an electronic transition [13]. In quantum mechanics, the principle characterizes the transition probability. The transition corresponding to the classical principle of conservation of nuclear coordinates and momenta has the highest probability. The physical reason is that a finite change of coordinates and momenta would require an infinitely high power and an infinitely large force, which are absent. Figure 6 illustrates the upper and lower potentials of the Hg_2 molecule and two wave functions. One function corresponds to motion with energy from the discrete spectrum, and the other function corresponds to atoms flying freely in opposite directions. One

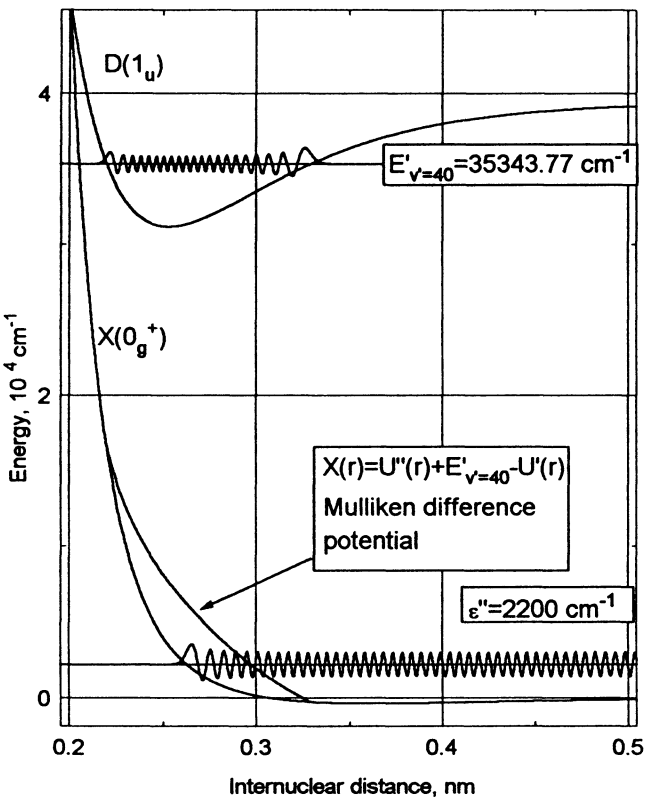

Fig. 6. The upper and lower potential curves of the Hg_2 dimer, the wave functions of the discrete and continuous energy spectra, and the Mulliken difference potential [1, 13].

can see that the transition from the lower classical turning point to the right-hand upper turning point does not correspond to the Franck–Condon principle. A higher probability is obtained for the vertical transition, which takes place for a internuclear distance of about 0.3 nm (the coordinate is conserved), from the point with a nonzero kinetic energy of the motion bounded on one side to a vibrational level, where the kinetic energy is conserved (the momentum is conserved). The difference

$$X(R) = U''(R) + E'_{\nu'} - U'(R) \tag{11}$$

forms the so-called Mulliken difference potential [1, 13] (its own for every ν') on which the most probable transitions from the lower state to the upper state due to photon absorption start. The energy of an absorbed quantum is equal to the difference

$$h\nu = E - X(R) \tag{12}$$

at the point corresponding to the highest transition probability. If one makes the necessary changes, the aforesaid relates to radiative bound-free transitions, as well.

Figure 7 once again illustrates the same functions as those presented in Fig. 6. The dashed line corresponds to the continuous spectrum of energy eigenvalues (the lower state, $\varepsilon'' = 2200$ cm^{-1}), and the solid line corresponds to the discrete spectrum ($\nu' = 40$). One can see from Fig. 7 that the functions have the same spatial periods for a internuclear distance of about 0.3 nm, which gives the coordinate of the most probable electronic transition. Moreover, Fig. 7 shows the product of wave functions (the integrand of the overlap

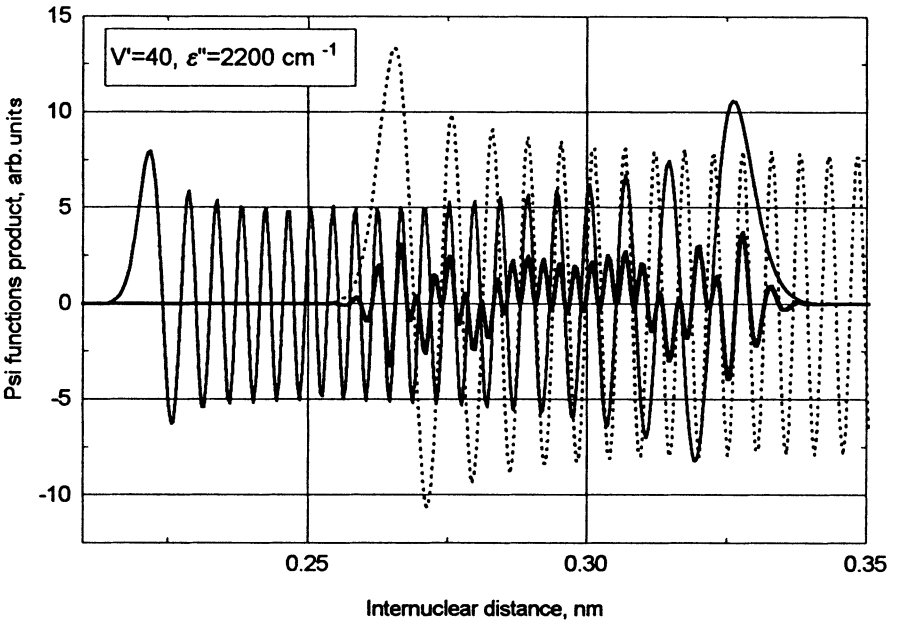

Fig. 7. Wave functions of the continuous ($\varepsilon'' = 2200$ cm^{-1}, dashed curve) and the discrete ($\nu' = 40$, solid line) energy spectra and the product of wave functions (thick solid line).

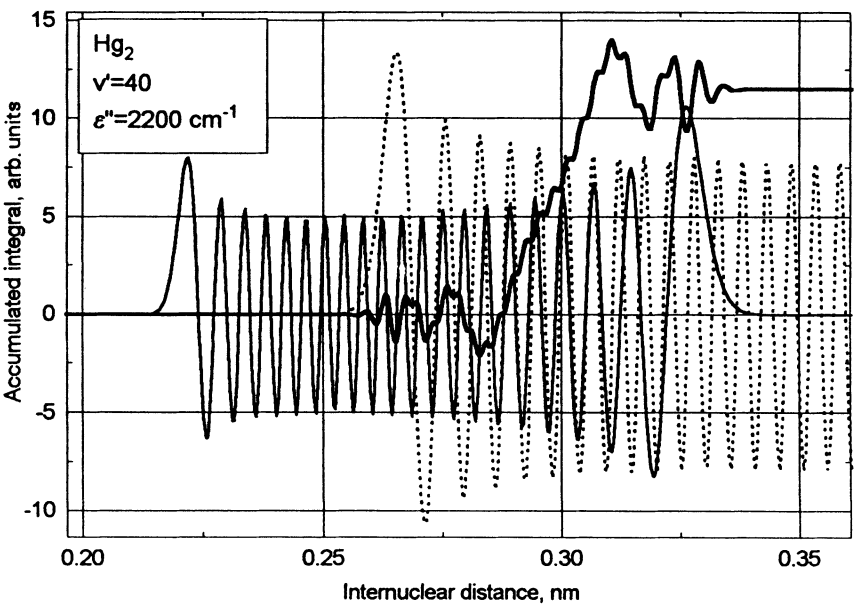

Fig. 8. The process of accumulation of the value of the Franck–Condon overlap integral (thick solid line), the rest is the same as in Fig. 7.

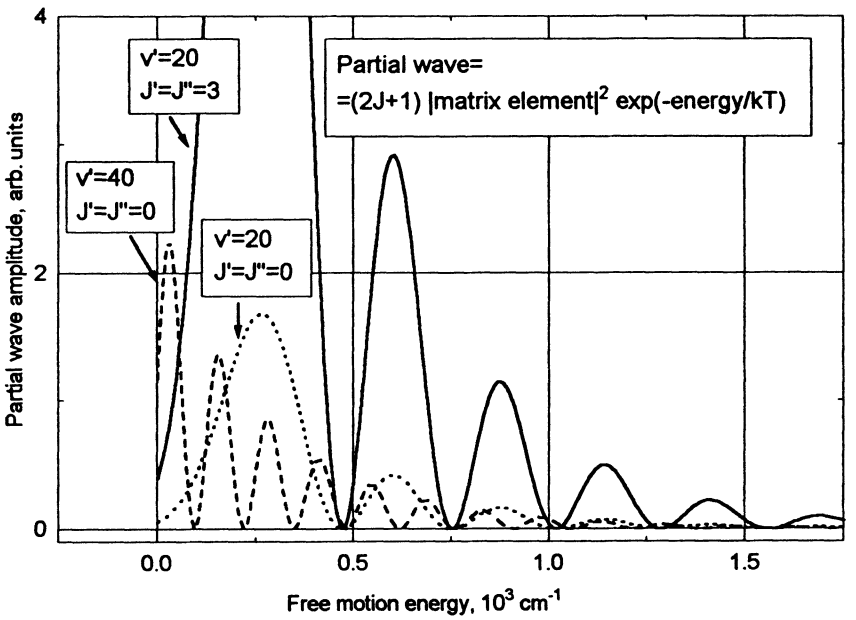

Fig. 9. Partial waves for different vibrational levels and rotational energies.

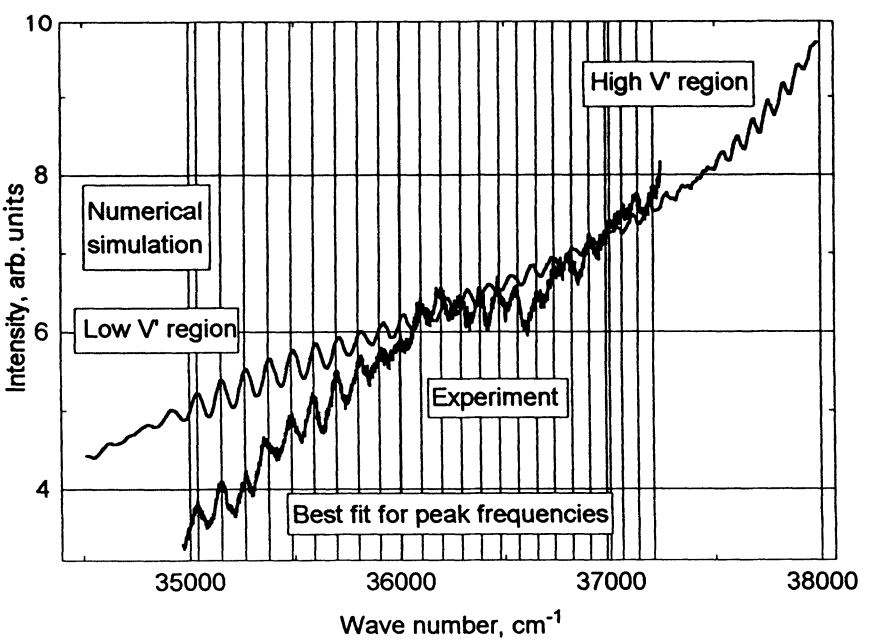

Fig. 10. Calculated and experimental absorption spectra for collisional Hg–Hg pairs.

integral, the thick solid curve). The curve oscillates near the coordinate of the most probable transition, but it remains positive there. Beyond the boundaries of this region, the curve oscillates with a change of sign. Note that the product vanishes outside the region where the functions overlap.

Figure 8 illustrates the same functions as those in Fig. 7, but together with a current value (the thick solid curve) of the integral $\int_0^R \phi_{\nu' J}\phi_{\varepsilon''}\, dR$. For $R \to \infty$, the latter integral represents the Franck–Condon overlap integral. One can see that the overlap integral is accumulated for the values of R corresponding to the most probable transition.

Figure 9 illustrates the partial waves calculated for several values of ν', ε'', and J by formula (3). The amplitude of a partial wave is proportional to $(2J+1)$, which is seen from the comparison of the curves in Fig. 9. The envelope of a partial wave decays in the direction of increasing translational energy ε'', which is caused by a decrease of the Boltzmann factor $\exp(-\varepsilon''/kT)$. Oscillations of a partial wave are caused by the change of phases of wave functions of the lower and upper states. A partial wave has a minimum for a phase difference of $\pi/4$. The phase difference of wave functions is not governed by the Franck–Condon principle. It is determined by the form of the potentials between which the electronic transition is observed. Summing the contributions of all partial waves, which are determined by formula (11), one obtains the absorption spectrum for the photoassociation of collisional pairs of atoms.

Figure 10 illustrates the calculated spectrum (the smooth curve) giving the best agreement with the experimental spectrum, which is shown by the noisy curve. The vertical lines in Fig. 10 mark the positions of peaks in the experimental spectrum. The positions of these lines are corrected in such a way that the difference of frequencies of the neighboring peaks monotonically decreases and forms a smooth frequency dependence.

The photoassociation spectrum was calculated for potentials of the following form. The lower potential was constructed according to the calculation data of [14], and the position of its minimum is shifted to the point R_e'' specified in [15]. Note that the Morse-type potential that was constructed using the data of [15] coincided on the right-hand side of R_e'' with the shifted potential from [14]. With the help of the factor $\{1+B''\exp[-\alpha''(R-2.2)]\}$, the Morse-type potential with parameters from [15] was made exactly coincident with the potential from [14]. The result of fitting is contained in the formula

$$\begin{aligned} U_J''(R) &= D_e''\{1+B''\exp[-\alpha''(R-2.2)]\}\{[1-\exp\beta''(R-R_e'')]-1\}+\frac{\hbar}{8\pi^2 c\mu\cdot 10^{-16}R^2}J(J+1), \\ \beta'' &= 10^{-8}\sqrt{8\pi^2\mu c\omega_e'' x_e h^{-1}} = 1.226827, \\ D_e'' &= 380, \quad \omega_e'' x_e = 0.253, \quad R_e'' = 3.63, \quad \alpha'' = 3.1\beta'' = 3.803313, \quad B = 1. \end{aligned} \tag{13}$$

In the calculations, the upper potential was used in the form of the Morse potential, and its parameters are taken from [15]. The values of these parameters are close to the values found in [16], but are somewhat different from them,

$$\begin{aligned} U_J'(R) &= D_e'\{[1-\exp\beta'(R-R_e')]-1\}+\frac{\hbar}{8\pi^2 c\mu\cdot 10^{-16}R^2}J(J+1)+E_a, \\ E_a &= 39424, \quad \beta' = 10^{-8}\sqrt{8\pi^2\mu c\omega_e' x_e h^{-1}}, \quad D_e' = 8260, \quad \omega_e' x_e = 0.45, \quad R_e' = 2.53. \end{aligned} \tag{14}$$

U_J, D_e, E_a, and $\omega_e x_e$ entering in (14) and (15) are measured in cm^{-1}, R and R_e are measured in angstroms (this accounts for the factors 10^{-16} and 10^{-8} in the formulas), α'' and β are measured in reciprocal angstroms, μ is the reduced mass in g, c is the speed of light in cm/s, and B is a dimensionless number.

The calculated spectrum coincides with the experimental spectrum in the low-frequency region from 35 000 to approximately 35 750 cm^{-1}. An attempt to obtain complete coincidence of the spectra by varying parameters of the Morse potential has not met with success.

The dependence $\mu(R)$ should be derived by the method proposed in [7]. At the given stage of calculations, $\mu(R)$ was assumed to be constant and, therefore, was not determined. Moreover, we assume that the wing of the resonant absorption line with $\lambda = 253.7$ nm is superimposed on the photoassociation spectrum for pairs of atoms. In our opinion, it will be possible in the future to determine the nature of resonant-line broadening, which represents the test of the theory of resonant-line broadening.

Acknowledgements

We are grateful to Dr. M. Dolg for the calculation data that were kindly placed at our disposal and to G. Z. Figen for ässistance in the work. This work was supported by the Russian Foundation for Basic Research under Projects Nos. 96-02-18950 and 96-15-96582 and in part by the US NSF.

References

1. J. Tellinghuisen, "The Franck-Condon principle in bound-free transitions," in: K. P. Lawley (Ed.), *Photodissociation and Photoassociation*, Wiley, New York (1985), p. 299.
2. E. U. Condon, *Phys. Rev.*, **32**, 858 (1928).
3. B. L. Borovich, V. S. Zuev, and D. B. Stavrovskii, *J. Quant. Spectr. Radiat. Transfer*, **13**, 1241 (1973).
4. J. H. Schloss, D. B. Geohegan, and J. G. Eden, *Bull. Am. Phys. Soc.*, **32**, 1230 (1988).
5. J. G. Eden, J. H. Schloss, D. J. Kane, et al., *Proc. SPIE*, **894**, 54 (1988).
6. J. H. Schloss, R. B. Jones, and J. G. Eden, *Chem. Phys. Lett.*, **191**, 195 (1992).
7. R. B. Jones, J. H. Schloss, and J. G. Eden, *J. Chem. Phys.*, **98**, 4317 (1993).
8. R. B. Jones, Ph.D. Thesis, University of Illinois, Urbana/Champaign, 1992.
9. I. S. Grigor'ev and E. Z. Meilikhov (Eds.), *Handbook of Physical Quantities* [in Russian], Énergoatomizdat, Moscow (1991).
10. M. F. Kink, R. A. Kink, M. V. Sel'g, and Yu. A. Maksimov, *Trudy Instituta Fiziki ÉSSR* [in Russian], (1987), Vol. 60, p. 127.
11. J. W. Cooley, *Math. Computation*, **15**, 363 (1961).
12. J. K. Cashion, *J. Chem. Phys.*, **39**, 1872 (1963).
13. R. S. Mulliken, *J. Chem. Phys.*, **55**, 309 (1971).
14. M. Dolg and H.-J. Flad, *J. Chem. Phys.*, **100**, 6147 (1996).
15. J. Koperski, J. B. Atkinson, and I. Krause, *Chem. Phys. Lett.*, **219**, 161 (1994).
16. A. Zehnacker, M. C. Duval, C. Jouvet, et al., *J. Chem. Phys.*, **86**, 6565 (1987).